

Title	Optimizing vanadium pentoxide thin films and multilayers from dip-coated nanofluid precursors
Authors	Glynn, Colm;Creedon, Donal;Geaney, Hugh;O'Connell, John;Holmes, Justin D.;O'Dwyer, Colm
Publication date	2014-01-16
Original Citation	Glynn, C., Creedon, D., Geaney, H., O'Connell, J., Holmes, J. D. and O'Dwyer, C. (2014) 'Optimizing Vanadium Pentoxide Thin Films and Multilayers from Dip-Coated Nanofluid Precursors', ACS Applied Materials & Interfaces, 6(3), pp. 2031-2038. doi: 10.1021/am4051102
Type of publication	Article (peer-reviewed)
Link to publisher's version	<a href="https://pubs.acs.org/doi/10.1021/am4051102">https://pubs.acs.org/doi/10.1021/am4051102</a> - 10.1021/am4051102
Rights	© 2014 American Chemical Society. This document is the Accepted Manuscript version of a Published Work that appeared in final form in ACS Applied Materials and Interfaces, copyright © American Chemical Society after peer review and technical editing by the publisher. To access the final edited and published work see <a href="https://pubs.acs.org/doi/10.1021/am4051102">https://pubs.acs.org/doi/10.1021/am4051102</a>
Download date	2024-02-22 03:17:50
Item downloaded from	<a href="https://hdl.handle.net/10468/6120">https://hdl.handle.net/10468/6120</a>



# UCC

**University College Cork, Ireland**  
Coláiste na hOllscoile Corcaigh

# Optimizing Vanadium Pentoxide Thin Films and Multilayers from Dip-Coated Nanofluid Precursors

Colm Glynn<sup>1,2</sup>, Donal Creedon<sup>1</sup>, Hugh Geaney<sup>1,2</sup>, John O'Connell<sup>1,2</sup>, Justin D.

Holmes<sup>1,2,3</sup> and Colm O'Dwyer<sup>1,2,4\*</sup>

<sup>1</sup> *Department of Chemistry, University College Cork, Cork, Ireland*

<sup>2</sup> *Micro & Nanoelectronics Centre, Tyndall National Institute, Lee Maltings, Cork, Ireland*

<sup>3</sup> *Centre for Research on Adaptive Nanostructures and Nanodevices (CRANN), Trinity College Dublin, Dublin 2, Ireland*

<sup>4</sup> *Materials & Surface Science Institute, University of Limerick, Limerick, Ireland*

## Abstract

Using an alkoxide based precursor, a strategy for producing highly uniform thin films and multilayers of  $V_2O_5$  is demonstrated using dip-coating. Defect free and smooth films of  $V_2O_5$  on different surfaces can be deposited from liquid precursors. We show how pinholes are formed due to heterogeneous nucleation during hydrolysis as the precursor forms a nanofluid. Using knowledge of instability formation often found in composite nanofluid films, and the influence of cluster formation on the stability of these films, we show how polymer-precursor mixtures provide optimum uniformity and very low surface roughness in amorphous  $V_2O_5$  and also orthorhombic  $V_2O_5$  after crystallization by heating. Pinhole and roughness instability formation during the liquid stage of the nanofluid on gold and ITO substrates is suppressed giving a uniform coating. Practically, understanding evolution pathways that involve dewetting processes, nucleation, decomposition or hydrolysis in complex nanofluids provides a route for improved uniformity of thin films. The method could be extended to improve the consistency in sequential or iterative multilayer deposits of a range of liquid precursors for functional materials and coatings.

## Introduction

Thin films grown from liquid precursors or solutions are often subject to sol-gel processes that influence uniformity.<sup>1</sup> Thin films, hybrid films and nanocomposite derivatives are important since their mode of processing often mimics that of polymer films, and often possess the properties of both the inorganic and organic phases. These different levels of complexity make controlled assembly or uniformity over a large dimension a major challenge of modern materials chemistry<sup>2</sup>. Thin films of alternative composite materials, those formed by the addition of nanoparticles of inorganic species to polymer films, i.e. nanofluids, offer the possibility of creating materials with features on the nano/microscale<sup>3</sup> with tunable properties due to nanoparticle–matrix, and nanoparticle–nanoparticle interactions.<sup>4-7</sup> While there has been significant research on the stability of thin polymer films, on particle aggregation, and the controlled assembly of monolayer and assemblies of nanoparticles<sup>8</sup>, the knowledge of the stability of films of hybrid materials, those where inorganic units are formed *in situ* by molecular precursors, is still being developed<sup>9</sup>.

Hybrid thin films, and indeed many physical and chemical vapour deposited thin films, rely on a high degree of uniformity and low roughness, and such degrees of morphology and composition control are difficult to produce in dip-coated or spin-cast liquid precursors due to their sensitivity to dewetting on various substrates. This difficulty is compounded by complications arising from the chemical decomposition and phase changes during hydrolysis or pyrolysis, which can often lead to a high density of inorganic units within the originally liquid film. Many of the classical inorganic solid state materials are formed using solid precursors and high temperature processes, which are often not compatible with the presence of organic groups because they are decomposed at elevated temperatures.<sup>2</sup> In some cases, this decomposition can prove useful when forming a metal oxide from a more complex organometallic or related derivative, and subsequent incorporation of polymeric/organic species can then influence growth.

Dewetting effect of liquids on surfaces can limit the spreading uniformity of liquid precursors, and applies to deposition on planar and non-planar substrates; the phenomenon is found with oil on a hot pan to more complex examples such as spin cast polymer films that are heated.<sup>10</sup> Research into bottom-up deposition methods is important for complex oxide films<sup>11-12</sup>, and directed self-assembly and block copolymer based techniques<sup>13</sup> augment well-known processes involving sol-gel or molecularly engineered clusters such as organometallic,

covalently or coordinatively designed precursors to help in the design of new functional materials, assemblies, arrays or coatings.<sup>14-16</sup>

Recently, several reports have shown that dewetting of thin liquid polymer films could be suppressed by the presence of ‘inclusions’, typically nanoparticles or small additives, with the resulting polymer film exhibiting spinodal character.<sup>5, 17</sup> Spinodal clustering and nucleation dewetting effects are characterized by specific pattern formation in surface films that are defined by a definite wavelength in their distribution.<sup>16, 18</sup> This wavelength is indicative of a perturbative instability that forms within the liquid resulting in a random orientation of features, where each feature is equidistant in all directions from the next-nearest neighbour.<sup>19</sup> These effects are likely in liquid alkoxides and similar precursors<sup>20</sup> that solidify in time to form another phase that is amenable to a thin film deposit. Recent papers identified definite control over polymer film smoothness and patterning by using Au nanoparticle networks on the surface of films, or C<sub>60</sub> fullerene structures within PMMA films, or even by the addition of colloidal quantum dot nanocrystals within polymer films as a composite.<sup>5, 10, 17, 21-22</sup> In all cases, beading of the polymer into typical Voronoi tessellations is prevented and several models have been advanced to explain these effects.<sup>9</sup>

During alkoxide hydrolysis, a system that is chemically well understood, the solidification during oxide formation is as a result of an ever increasing density and association of oxide entities within a liquid that increases in viscosity until a solid film forms.<sup>23</sup> We report on such a system and show that these effects are not only similar to nanoparticle-loaded liquid polymer films that do not fully dewet a surface, but help to understand the underlying process that defines the hydrolysis of an alkoxide of vanadium to vanadium oxide, and influences the resulting morphology of the nominally layered material.<sup>24-25</sup> The production of devices from thin films of amorphous metal oxides has been recently studied and new techniques are always being examined for their synthesis.<sup>26-28</sup>

Here, we demonstrate that the well-known alkoxide of the transition metal vanadium, in liquid form on a surface to which it wets, undergoes a mechanism of competitive nucleation dewetting and solidification via hydrolysis that influences and defines the final structure and morphology of the film.<sup>20, 29</sup> Thin films of vanadium pentoxide (V<sub>2</sub>O<sub>5</sub>) have been used in the production of polymer solar cells as interfacial buffer layers<sup>30</sup> and for bolometer applications,<sup>31</sup> but also for electronic materials<sup>32</sup>, optical materials<sup>33</sup>, charge storage electrodes for batteries<sup>34</sup>, and in ionic sensing based on their layered structure and oxidation state.<sup>35</sup> The formation of thin films of V<sub>2</sub>O<sub>5</sub> for devices using a dip-coating technique would be beneficial for large area

coverage with high uniformity often required for optical materials and functional coatings. By adjusting the alkoxide precursor and the crystallisation procedure, thin films of vanadium oxide with different oxidative states can be produced.<sup>36-37</sup> By utilizing the deposition techniques in this work, thin films with a smooth and uniform morphology over large areas are possible. This low-roughness characteristic would be beneficial for materials such as vanadium dioxide (VO<sub>2</sub>), which has recently been shown to act as a disordered metamaterial with blackbody-like thermal emissivity<sup>38-39</sup> and thermochromic<sup>40-41</sup> properties.

Many physical and chemical vapour deposition processes have difficulty controlling the stoichiometry of vanadium oxides<sup>42</sup> and in general, non-planar substrates cannot be uniformly coated by these methods. The development of atmospheric pressure deposition technologies highlights the importance of low-cost and high-throughput processing with open air systems, which are important for many industrial applications.<sup>43</sup> However, depending on the desirable surface morphology of the film for each device, it is important to examine the formation effects of the thin films on different substrates and the techniques to limit unwanted morphologies from forming during deposition, especially when using liquid-based methods.<sup>44</sup>

The potential similarity to polymer-NP composited films inspired the search for the underlying mechanism of this classic phase formation process and to develop a protocol allowing optimization of the uniformity of thin films from liquid based precursors that solidify through hydrolysis. The addition of polyethylene glycol (PEG) or an increase in the viscosity of the alkoxide mixture can minimize pinhole formation and non-uniformities in coated thin films.

## **Experimental**

Thin vanadium oxide (V<sub>2</sub>O<sub>5</sub>) films was synthesised from vanadium (V) triisopropoxide OV(OCH(CH<sub>3</sub>)<sub>2</sub>)<sub>3</sub> purchased from Sigma-Aldrich. The alkoxide was mixed by volume with isopropyl alcohol and deionised water at a ratio of 1000:10:1 (IPA : alkoxide : water) to produce a low concentration precursor. The precursor was stored with 4 Å molecular sieves from Sigma-Aldrich to prevent hydrolysis prior to use.

Two deposition techniques were used for preparing the samples. Drop casting was used to deposit irregular films of V<sub>2</sub>O<sub>5</sub> while dip coating was used to form uniform thin films. Dip coating was performed using a PTL-MM01 desktop dip coater. A withdraw rate of 150 mm/min was used for depositing the thin films in this work.

Thin films were deposited onto both Au and ITO coated glass substrates due to their prevalence as current collectors for applications involving  $V_2O_5$ . Borosilicate glass cantilevers, 60 mm in length and 3 mm in width, were coated with a 10 nm Ti adhesion layer and a 250 nm Au layer by high vacuum thermal evaporation. The Au coated substrates were thermally annealed at 650 °C for 90 s prior to deposition of the precursor to produce larger Au grains and prevent delamination occurring during the thin film deposition. The growth in grain size due to annealing is shown in Fig. S1 (a,b). ITO coated glass was purchased from Sigma-Aldrich and cleaved into strips 25 mm in length and 3 mm wide for direct comparison to the Au substrates. Multiple coatings can be performed during dip coating to produce films with a desired thickness. To examine the changes between subsequent layers, “staircase” samples (see Fig. 1a) were prepared by successively dip-coating thin films with shorter film lengths on top of underlying layers such that the morphology of each successive layer could be examined on a single sample for direct comparison. After deposition, the samples are UV-Ozone treated for 30 minutes in a Novascan UV ozone system to remove any organics that remain from the precursor.

Surface morphologies were examined using scanning electron microscopy (SEM) and atomic force microscopy (AFM). SEM analysis was performed on an FEI Quanta 650 FEG high resolution SEM equipped with an Oxford Instruments X-MAX 20 large area Si diffused EDX detector. Images were collected at an operating voltage of 10-20 kV. AFM was used to analyse the surface topography and roughness of the prepared samples. Scans were performed on a Park XE-100 AFM system in non-contact mode with SSS-NCHR enhanced resolution tips, the XY and Z resolution are ~ 2 nm and 0.05 nm respectively.

To determine the phase of the films post-crystallisation, Raman scattering spectroscopy was collected with a Renishaw InVia Raman spectrometer using a 514 nm 30mW Argon Ion laser, spectra were collected using a RenCam CCD camera. The beam was focused onto the samples using either a 20×/50× objective lens. X-Ray Diffraction (XRD) analysis was performed using a Phillips Xpert PW3719 diffractometer using Cu  $K\alpha$  radiation (40 kV and 40 mA) scanned between 10° - 40°.

X-Ray photoelectron spectroscopy (XPS) spectra were acquired on an Oxford Applied Research Escabase XPS system equipped with a CLASS VM 100 mm mean radius hemispherical electron energy analyser with multichannel detectors in an analysis chamber with a base pressure of  $3.0 \times 10^{-9}$  mbar. Survey scans were recorded between 0-1100eV with

a step size of 0.7 eV, dwell time of 0.5 s and pass energy of 100 eV. Core level scans were acquired at the applicable binding energy range with a step size of 0.1 eV, dwell time of 0.5s and pass energy of 20 eV averaged over 10 scans. A non-monochromated Al-K $\alpha$  X-ray source at 150 W was used for all scans. All spectra were acquired at a take-off angle of 90° with respect to the analyser axis.

Structure factors used for examining the spatial arrangement of pinholes within films were acquired by carefully thresholding digital images and obtaining fast Fourier transforms (FFTs). Random distributions of features without any definitive wavelength in position give a decaying intensity from the maximum intensity (000) central mode.

## Results and Discussion

Thin films of V<sub>2</sub>O<sub>5</sub> were prepared using two deposition techniques: Drop casting and dip coating. During drop casting, the precursor is dropped onto the substrate to initiate the hydrolysis step, and is unconstrained. The length of time for the hydrolysis step to completely form a V<sub>2</sub>O<sub>5</sub> solid film is dependent upon the alkoxide concentration. While still in liquid form, the precursor can spread across the surface of the substrate (unlike the case of dip-coating) until the hydrolysis is complete. Unlike most transition metal alkoxides that form particulate structures, the layered molecular structure of vanadium oxide allows a dominant layering of the crystal structure parallel to the substrate.<sup>25, 45</sup> Recently it has been shown that dip-coating of vanadium alkoxide precursors can result in surface cracking of the thin films.<sup>37</sup>

During dip-coating the substrate is drawn from the precursor at a controlled rate with the hydrolysis occurring once exposed to air. The hydrolysis of the alkoxide to its oxide after dip-coating occurs rapidly so that an amorphous V<sub>2</sub>O<sub>5</sub> thin film is formed and the increased dewetting and beading normally experienced by the drop casted liquid thin films is prevented.

Figure 1(a) is an SEM image of the surface of a thin film of as-deposited V<sub>2</sub>O<sub>5</sub> on an Au substrate. The sample was deposited in a staircase configuration, depicted in the schematic in Fig. 1(a) which is composed of iterative dip coats after hydrolysis has occurred to form a multi-layered deposit. The low magnification SEM image shows the film surface and interfaces for the Au substrate and the first two successive layers of V<sub>2</sub>O<sub>5</sub>. The interfacial regions are highlighted for visual aid. Each successive layer thickness of V<sub>2</sub>O<sub>5</sub> is measured to be 15 – 18 nm. The AFM insets show the surface morphology of each of the surfaces respectively. The

first dip-coated layer of  $V_2O_5$  on Au exhibits a similar morphology to the Au grains while the AFM image shows the formation of pinholes on the surface of layer 2. The AFM surface image of layer 2 is that of a typical  $V_2O_5$  film formed on top of a previously formed  $V_2O_5$  film on an Au substrate, i.e. the second, third, etc. layers. Small 25 – 35 nm diameter pinholes, which are between 6 and 10 nm deep, were revealed by AFM analysis. These features are characteristic of oxide thin film formation from liquid alkoxide precursors based on our examinations. The pinholes are only apparent on the AFM image; their shallow depth and the secondary electron intensity from the underlying Au substrate beneath the film reduce the visibility of small defects in the  $V_2O_5$  film from SEM images as can be seen in Fig. S2.

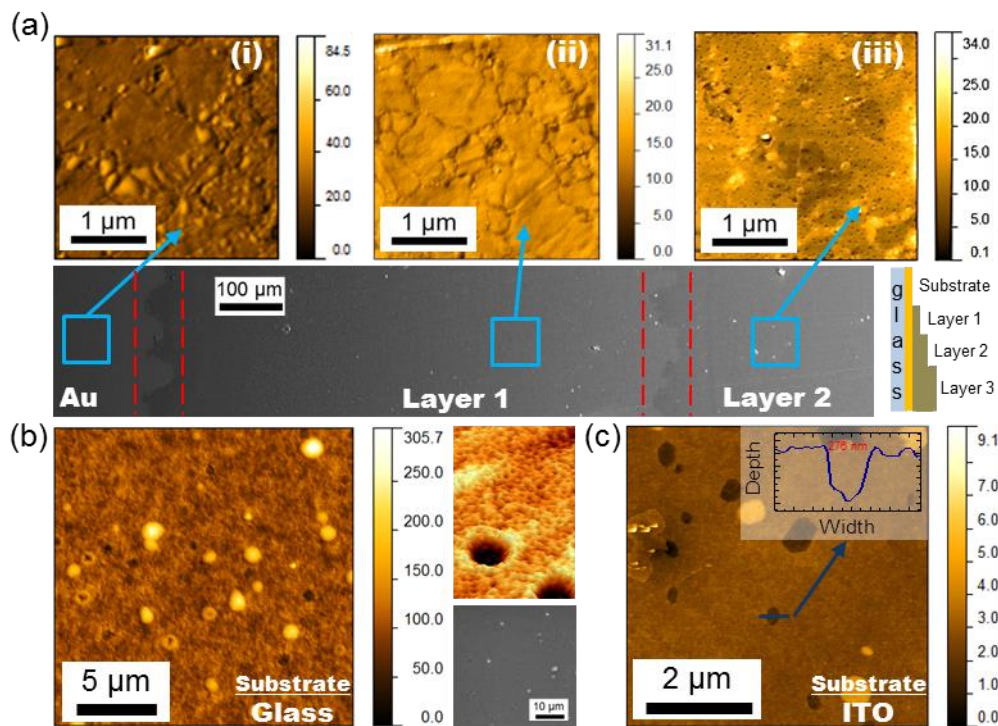


Figure 1. (a) SEM of as-deposited  $V_2O_5$  film on an Au substrate with the interfaces highlighted between each successive layer. AFM images showing the morphology of the (i) Au substrate, (ii) first layer of  $V_2O_5$  film and (iii) second layer of  $V_2O_5$  film with formation of pinholes visible. The schematic architecture of a ‘staircase’ thin film sample. (b) AFM and SEM images of  $V_2O_5$  drop casted on glass. (c) AFM image of dip-coated  $V_2O_5$  film on an ITO substrate. Pinholes of different distributions and sizes are present in these samples compared to films formed on Au substrates. The unit for the AFM sidebars is in nm.

The as-deposited surface images from AFM and SEM for drop casted films on glass are shown in Fig. 1(b). Due to the increased hydrolyzation time involved in drop casting (compared to dip-coating of thinner films),  $V_2O_5$  films formed on different substrates by drop casting share similar morphologies. Both surface bound hillock features and pinholes are



present in the thicker drop casted film in Fig. 1(b) as seen from both the top down and AFM images, confirmed by SEM showing the presence of hillock features on the surface. The surface roughness of the drop casted film from the AFM images displays a labyrinthine topology that is similar to spinodal instability (buckling and undulations) effects<sup>10, 22</sup> seen in polymer thin films, and we find that such features of fully hydrolysed amorphous  $V_2O_5$  films are seen when thicker drop cast films are examined.<sup>19</sup>

The formation of pinholes that are similar to nucleation dewetting effects in composite liquid polymer films, is also observed on dip-coated  $V_2O_5$  thin films formed on ITO substrates shown in Fig. 1(c). The pinholes formed on the ITO have a characteristically larger size and shape compared to those formed on the rougher, granular Au surface. The pinholes formed on ITO have a lower distribution compared to those on Au. The pinholes on ITO are also formed from the first layer and maintained in subsequent dip-coated layers. As-deposited amorphous  $V_2O_5$  thin films deposited on ITO also contain hillocks of material on their surfaces, as seen in Fig. 1(c); hillock formation is a common trait between the thin films formed on both Au and ITO substrates. It is not entirely clear from measurement of multilayer deposition if the movement of material during pinhole formation is related to the density and size of hillocks, but typically, their density and position is not spatially correlated to the distribution of the pinhole features in the first and subsequent layers.

The Au substrates are measured to have a greater rms roughness (5.43 nm) than the transparent ITO substrates (2.03 nm). The roughness of the amorphous thin films formed on the Au and ITO substrates are 2.61 nm and 0.68 nm respectively: for both types of films the rms roughness of the amorphous thin films is less than that of the respective metal or ITO substrates.

During the hydrolysis step, the liquid film forms clusters of hydrolysed amorphous  $V_2O_5$  which are suspended in the liquid precursor until hydrolysis is complete and the solid film has formed. This effect may be described as a thin film mixture where the solvent and solute are the liquid precursor and hydrolysed amorphous  $V_2O_5$  respectively, similar to Class I hybrid nanocomposite blends. The deposit is somewhat analogous to network modifiers in sol-gel processes involving blends of molecular building blocks, but here, these building blocks form *in-situ* during the chemical change.<sup>46</sup> Similar systems have been examined in the case of thin polymer films containing mixtures and suspensions.<sup>9</sup> Recently, a gradient dynamics description was proposed for films of mixtures and suspensions involving a concentration-

dependent wettability for liquid films containing suspensions.<sup>9</sup> The model details an ability of a film containing a suspension to modulate its thickness and concentration simultaneously, giving rise to feature formation. In the present case, the increasing viscosity during hydrolysis to a solid oxide from its alkoxide complicates the comparison to particle-loaded liquid polymer films, but motivated the experimental investigation into improving the uniformity in thin film formation by suppressing instabilities that can form in the thin film in its liquid state prior to solidification by hydrolysis.

Figure 2(a-b) shows the morphological characteristics of the two types of pinholes formed on Au and ITO substrates respectively. The pinholes formed on Au substrates are generally smaller (in width) but consistently deeper (6 – 9 nm), compared to shallower (3 – 5 nm) pinholes in  $V_2O_5$  films on ITO. On ITO the pinholes are predominantly non-circular with a significantly larger width to those on Au. As the precursor hydrolyses and solidifies after deposition, the form of dewetting process, including instabilities caused by lateral variations in nanoscale oxide cluster density throughout the films, thickness variations and changes in material parameters during hydrolysis to its oxide form, are halted by solidification leaving a solid film with a random distribution of pinhole defects. These defects are also observed on secondary, tertiary and further sequential layers of the thin film multilayer.

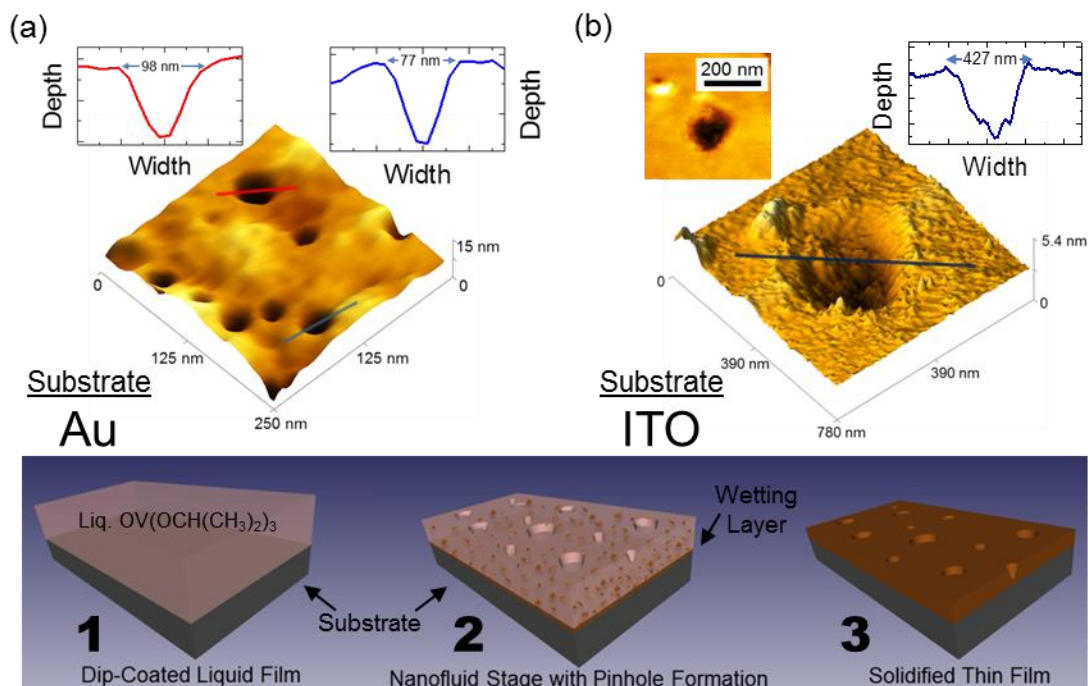


Figure 2. AFM images, topology and depth profiles for pinholes formed on (a) Au and (b) ITO substrates. The schematic illustrates the various phases of film hydrolysis: (1) dip-coating of liquid precursor that (2) develops a hydrolysed wetting layer to the surface with the continual

formation of oxide clusters within the hydrolysing films which leads to the formation of (3) a roughened, pinhole-containing solid film.

The distribution of the pinhole diameters formed on Au is shown in the graph for Fig. 3(a), the pinholes form in varying sizes with an average diameter (longest axis) of 27.3 nm. Statistical analysis of AFM images shows that the pinholes cover less than 8% of the total surface area for both types of substrates (this information is summarized in Table S1).

The distribution of the pinholes on Au was examined using Fast Fourier Transforms (FFT) of the AFM data. The FFTs were performed to ascertain any periodicity in the distribution of the pinholes, the method used in calculating the FFTs of the pinholes is outlined in Fig. S3. The FFTs for the two layers shown in Fig. 3(b-c) indicate that the pinholes are randomly distributed on the surface of both Au and ITO surfaces due to the lack of evidence for a characteristic inter-feature wavelength expected in samples that undergo defined instabilities, such as spinodal decomposition, or influences from lateral concentration variations<sup>17</sup> (Marangoni and other instabilities that assume the oxide clusters are mobile). Pinhole formation in liquid polymer films that contain nanoscale inclusions that prevent complete dewetting typically result from heterogeneous nucleation. Pinholes formed through this mechanism that open right down to the substrate become pinned in liquid films, but typically are not found in the present case even during the early stages when the dip-coated film is liquid. We believe this effect is due to a very thin wetting layer that instantaneously hydrolyses due to the presence of adsorbed water molecules on the substrate. AFM measurements in all cases consistently show a lesser pinhole depth compared to the average final film thickness.

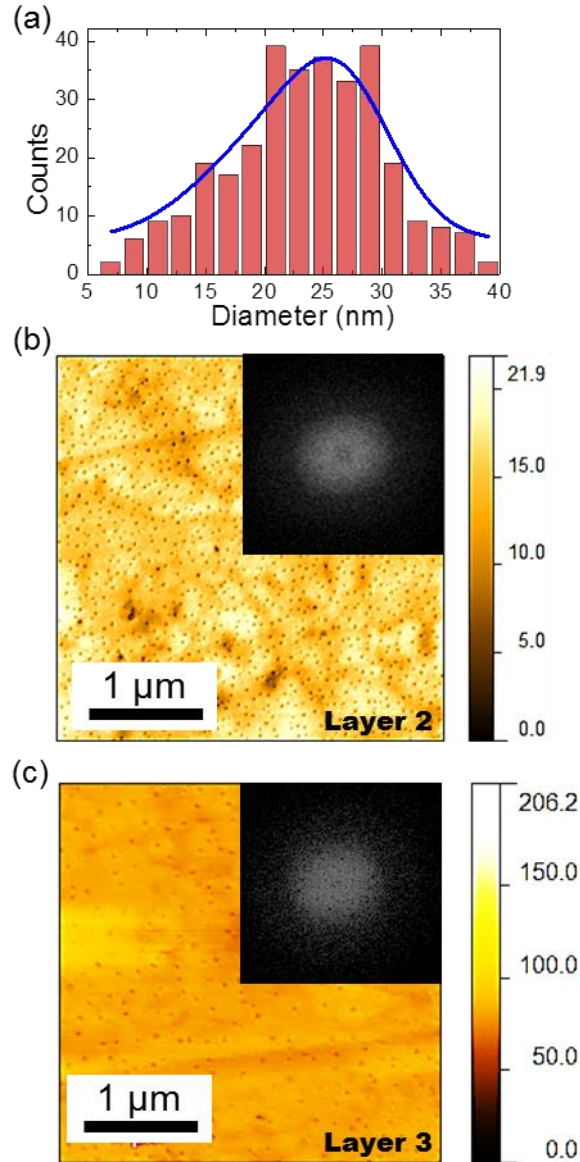


Figure 3. (a) Diameter distribution of pinholes formed on the surface of an Au substrate. (b-c) AFM surface image and corresponding FFT of pinhole distribution for two subsequent layers of  $V_2O_5$  thin films on Au. The FFTs illustrate the random distribution of the pinholes.

To examine the influence of crystallization on the morphology of thin films, the  $V_2O_5$  films were crystallized in air using a convection oven at 300 °C for 12 hours. The surface of the films was examined post-crystallisation to ascertain the changes to the thin film morphology after the phase change from amorphous to orthorhombic  $V_2O_5$ .<sup>34,47</sup> Figures 4(a-b) show the AFM and SEM surface images of the crystallized  $V_2O_5$  films on both Au and ITO substrates respectively. In both cases crystallites of  $V_2O_5$  form on the surface of the thin films with an average height of 31.7 nm and 36.8 nm on both Au and ITO respectively. In the case

of the thin films on Au, the pinholes are still apparent on the AFM images while their average depth is reduced to 4.8 nm. The rms roughness of the orthorhombic  $V_2O_5$  thin films on Au and ITO is 9.7 nm and 5.9 nm respectively. The increase in roughness is predominantly related to the changes caused by crystallization, the greatest roughening found for thin films on Au.

An XPS spectrum, Fig. 4(c), was acquired for both an as-deposited amorphous and crystallized single layer thin film of  $V_2O_5$  deposited on an ITO substrate. The as-deposited and crystallised spectra show the expected  $V2p_{3/2}$ ,  $V2p_{1/2}$  and  $O1s$  XPS peaks for  $V_2O_5$  at 517.5 eV, 524.6 eV and 530.6 eV respectively.<sup>48</sup> The presence of the oxygen XPS peak at 532.6 eV is not attributed to the formation of another vanadium oxidative state in the film.<sup>48-49</sup> The O 1s core-level emission is due to contributions from the ITO conductive layer and the  $SiO_2$  substrate underneath the  $V_2O_5$  thin film.<sup>50-51</sup> The low intensity 3d core-levels peaks for Sn and In are shown in Fig. S4. The presence of XPS peaks for the substrate underneath the thin film is due to the thinness of the single layer of  $V_2O_5$ . The XPS study demonstrates that the  $V_2O_5$  films are free of surface contaminants from the alkoxide precursor or other sources. Additionally, the oxidation state for as-deposited and crystallized films remains unchanged.

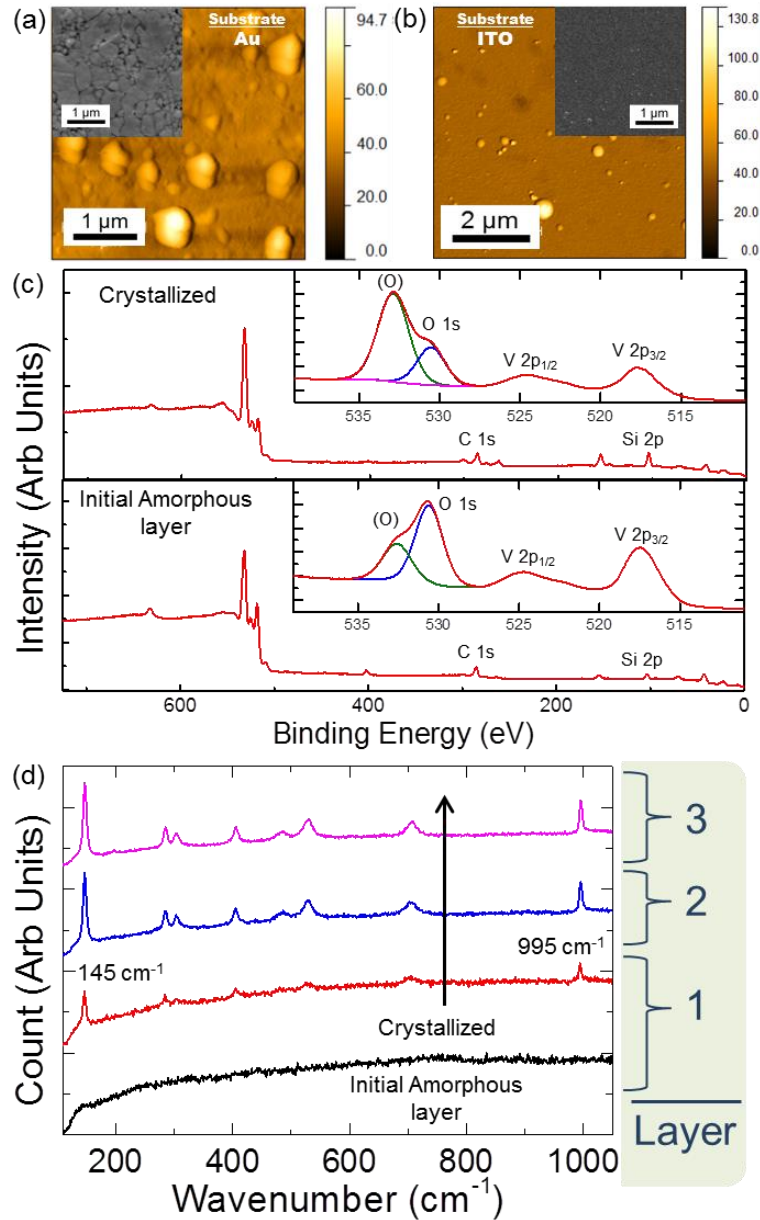


Figure 4. Post-crystallization AFM and SEM (insets) images of  $V_2O_5$  thin films on (a) Au and (b) ITO substrates. The images show the formation of dispersed crystallites on the surface. (c) XPS spectra of amorphous and crystalline  $V_2O_5$  thin films on ITO showing the contribution of photoelectron emission from the underlying substrate due to the thinness of the film. (d) Raman scattering spectra of the as-deposited and crystallized films for successive films in the multilayer.

Figure 4(e) shows the Raman scattering spectra of the  $V_2O_5$  thin film coatings on Au before and after crystallization. The as-deposited thin film is amorphous  $V_2O_5$ , thus no specific phonon modes from the known V-O bond structure are found. Post-crystallization, the characteristic vibrational peaks for orthorhombic  $V_2O_5$  are present, and identical to that

expected from the lamellar phase for the material.<sup>52-53</sup> Multilayers of  $V_2O_5$  from iterative dip-coating also crystallize to orthorhombic  $V_2O_5$ , a stoichiometric phase that can be difficult to control using CVD, ALD and related physical vapour deposition methods. Conventional XRD was found to be inadequate in determining the crystal structure of the thin films. To correlate the Raman scattering spectra of the thin films to X-ray diffraction characteristics of  $V_2O_5$ , a thick film with a high surface area was produced by drop casting the precursor followed by crystallization. The (001) reflection for orthorhombic  $V_2O_5$  at  $\sim 20.5^\circ$  is shown in Fig. S5(a) and can be correlated to the Raman scattering spectra for orthorhombic  $V_2O_5$  in Fig. S5(b). Additionally, the uniformity in the morphology and consistent low roughness is remarkable for single and multilayer deposits on metallic and transparent conducting oxide (TCO) substrates.

Most polymers are immiscible with alcohols, particularly alcohols released during the hydrolytic sol-gel process and phase separation becomes a problem for uniform film coverage. Utilizing polymers that are soluble with decomposition alcohols as the liquid film hydrolyzes as a cluster-containing solid film, could potentially alleviate concentration variations and unwanted structuring from these effects, which are detrimental to functional electronic and optical coatings and films.<sup>54</sup>

As with liquid polymer films, a change in molecular weight of the precursor and the viscosity fundamentally affects processes such as dewetting, nucleation, demixing and phase separation, and in those cases are fundamentally linked to gelation via hydrolysis where the material essentially contains internal ‘pores’ that allow the release of the alcohol, and eventual solidification. Furthermore, this uniformity should also be maintained when crystallizing the thin films after deposition. To improve film consistency and suppress pinhole formation through nucleation effects, a precursor was prepared utilizing polymer-assisted  $V_2O_5$  thin film synthesis. The hydrophilic and alcohol-soluble polyethylene glycol (m.w. = 400 g/mol) was added to the precursor to bind the amorphous  $V_2O_5$  clusters together during the hydrolysis of the liquid precursor stage. The AFM surface images for the corresponding  $V_2O_5$  thin films, pre- and post-crystallization, formed using this polymer-assisted alteration are shown in Fig. 5(a).

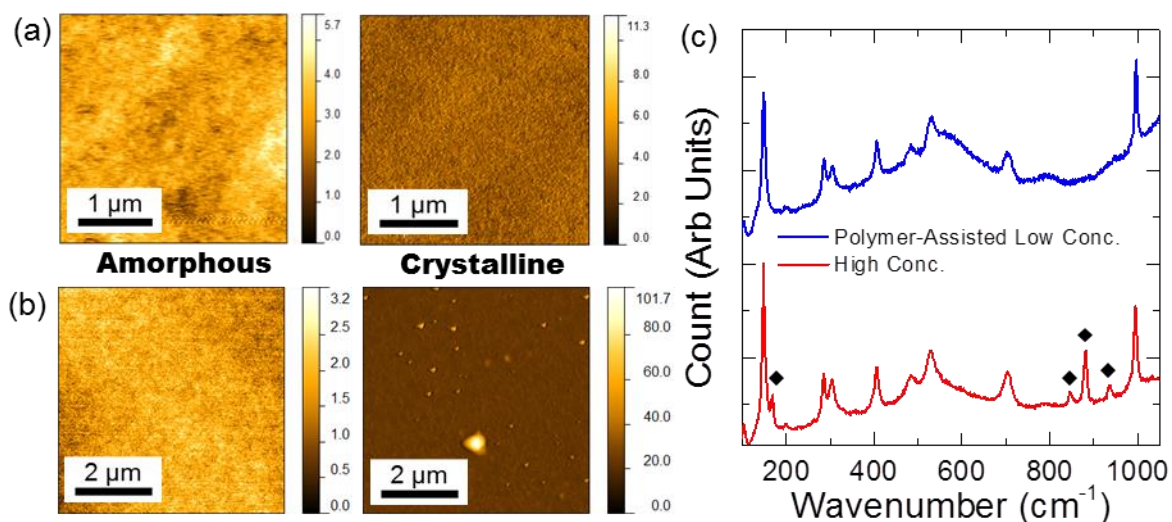


Figure 5. AFM images pre- and post-crystallization for (a) polymer-assisted low concentration and (b) high concentration  $V_2O_5$  thin films formed on ITO. (c) Raman scattering spectra showing the formation of crystalline orthorhombic  $V_2O_5$  from both films. The peaks marked with diamonds are due to the layered structure of the films and the presence of small amounts of  $VO_2$ . The broad background seen in the polymer-assisted spectra between  $400\text{ cm}^{-1} - 700\text{ cm}^{-1}$  is due to the thinness of the film and the interaction with the ITO and glass substrate.

The resultant thin films have a uniform surface morphology and no evidence of pinhole formation is found. The Raman scattering spectrum, included in Fig. 5(c), shows the formation of orthorhombic  $V_2O_5$  after the thermal treatment. The surface rms roughness for the amorphous and orthorhombic polymer-assisted  $V_2O_5$  thin films is  $0.57\text{ nm}$  and  $0.74\text{ nm}$  respectively. Crystallization also calcines the mixture, removing the organic component and from Fig. 5; the organic phase decomposition does not adversely affect the morphology of the thin films. Additionally, during the hydrolysis, the PEG is soluble in evaporating alcohols and may aid in preventing material cracking, and promote a smoothing of the surface topology by preventing instabilities forming within the hydrolysing film. By utilizing the polymer-assisted blend, a uniform non-defective thin film of orthorhombic  $V_2O_5$  was prepared with a surface roughness an order of magnitude below that of thin films prepared without the addition of a polymer.

A secondary method for smoothing the surface topology is demonstrated by increasing the concentration of the precursor in the IPA-alkoxide mixture. This decreases the hydrolyzation time of the liquid film, and is found to suppress the formation of pinholes in the initial amorphous layer. The decrease in hydrolyzation time does increase the thickness of the single layer to  $35 - 40\text{ nm}$  per layer. As in the case with the polymer-assisted films, the resultant



thin films have a uniform surface morphology with a low rms roughness of 0.56 nm. However, after crystallization of higher concentration alkoxides (without PEG), large crystallites form on the surface and the rms roughness increases to 5.61 nm, which correlates to similar crystallization behaviour of the thin films without polymer addition. Raman scattering spectra in Fig. 5(c) show the characteristic vibrational peaks for orthorhombic  $V_2O_5$ , however, the presence of extra peaks at  $168\text{ cm}^{-1}$ ,  $846\text{ cm}^{-1}$ ,  $880\text{ cm}^{-1}$  and  $935\text{ cm}^{-1}$ , are attributed to contributions from the layered structure, or the presence of  $VO_2$  in the polymer-assisted thin films.<sup>55</sup>  $VO_2$  phases in thin films with textured surface have been grown from vanadium triisopropoxides under atmospheric pressure chemical vapour deposition (APCVD).<sup>33, 56-57</sup> While increasing the concentration of the precursor can halt the formation of pinholes and surface texturization from grains or nanoscale clusters in  $V_2O_5$  thin films at the nanofluid stage, the polymer-assisted method with more dilute alkoxide mixtures has the additional benefits of lower single layer thicknesses ( $V_2O_5$  only) and a very low surface roughness both before and after crystallization.

## Conclusions

Using an alkoxide based precursor and cost-effective dip-coating techniques, a rational strategy for the deposition of highly uniform thin film and multilayers of  $V_2O_5$  on a range of surfaces from liquid based precursors was demonstrated. The nature of hydrolysis of the layered material  $V_2O_5$  from its alkoxide has been shown to strongly influence the uniformity of thin films formed on Au and ITO substrates as single thin films and as thin film multilayers. Utilizing knowledge of instability formation in liquid thin films and the influence of clusters as a nanofluid on the stability of such films, the addition of polymers to the nanofluid drastically improves uniformity and smoothness for amorphous and crystalline phases of  $V_2O_5$  that can exceed that of physical and chemical vapour deposition methods.

The choice of substrate was found to have an effect on the type of pinholes formed. Small diameter pinholes with a high distribution are found on for  $V_2O_5$  films deposited on granular sputtered Au films, while those on ITO substrates have a large irregular size and lower distribution. AFM and electron microscopy confirmed pinhole formation in addition to a specific surface roughness that is correlated to heterogeneous nucleation dewetting effects caused when the alkoxide was in its liquid state. The surface roughness and wettability of the

substrates combined with the alkoxide to solvent ratio of the precursor are associated with the formation of the pinholes.

The primary difference between the two systems is that due to the hydrolysis effect experienced by the alkoxide precursor in the formation of the  $V_2O_5$ , the thin films produced solidify prior to the full dewetting and nucleation process can finish as found in polymer films. To reverse the formation of pinholes and hillocks in the  $V_2O_5$ , a polymer assisted synthesis using PEG altered the hydrolysis and gelation point of the nanofluid during solidification such that an ultra-smooth surface is possible without pinholes or roughness linked to instabilities from the liquid stage that becomes frozen-in upon solidification.

Practically, understanding evolution pathways that involves dewetting processes, nucleation, decomposition or hydrolysis that includes evaporation in complex nanofluids gives routes to improved surface coverage of useful stoichiometry of  $V_2O_5$  using dip-coating. While further theoretical work would strongly benefit additional experimental investigations to fully explain the phenomenon, the method may prove useful for deposition of thin uniform films for a variety of applications on planar or possibly non-planar substrates (which form shadows and blank regions in many vapour-phase depositions). Dip-coating or spin casting liquids precursors and nanofluids can be extended to improve the consistency in sequential or iterative multilayer deposits of hybrid materials, and provides a liquid-based route for crystallized thin vanadium oxide films with exotic thermal, electrical and optical properties. In parallel with CVD and related plasma based deposition methods, such control of thin film uniformity gives another alternative for atmospheric pressure, open air methods for uniform films or coatings.

### **Supporting Information**

SEM analysis of the gold substrate grain size with annealing, and the method for identifying thin, electron beam-transparent thin films on gold. Information the pinhole diameter distribution and area covered is provided together with the method for producing FFTs AFM imagery. Additional XRD and Raman scattering measurements of bulk and thin film  $V_2O_5$  is provided together with XPS of In and Sn core-levels. This material is available free of charge via the internet at <http://pubs.acs.org/>.

## **Corresponding Author**

Email: [c.odwyer@ucc.ie](mailto:c.odwyer@ucc.ie); Tel: (0)21 4902732; Fax: (0)21 4274097

## **Acknowledgements**

C.G. acknowledges the support of the Irish Research Council under awards RS/2011/797. This research has received funding from the Seventh Framework Programme FP7/2007-2013 (Project STABLE) under grant agreement n°314508. C.O.D. acknowledges support from the UCC Strategic Research Fund, and from the Irish Research Council New Foundations Award. This work was also supported by SFI under the National Access Programme (NAP 417).

## References

1. Brinker, C. J.; Frye, G. C.; Hurd, A. J.; Ashley, C. S., Fundamentals of sol-gel dip coating. *Thin Solid Films* **1991**, *201*, 97-108.
2. Ozin, G. A., Arsenault, A. C. Cademartiri, L. *Nanochemistry: a chemical approach to nanomaterials*, 2nd ed; RSC Publishing: Cambridge, 2009.
3. Valenzuela, C. D.; Carriedo, G. A.; Valenzuela, M. L.; Zuniga, L.; O'Dwyer, C., Solid State Pathways to Complex Shape Evolution and Tunable Porosity during Metallic Crystal Growth. *Sci. Rep.* **2013**, *3*.
4. Mukherjee, R.; Das, S.; Das, A.; Sharma, S. K.; Raychaudhuri, A. K.; Sharma, A., Stability and Dewetting of Metal Nanoparticle Filled Thin Polymer Films: Control of Instability Length Scale and Dynamics. *ACS Nano* **2010**, *4*, 3709-3724.
5. Amarandei, G.; O'Dwyer, C.; Arshak, A.; Corcoran, D., Fractal Patterning of Nanoparticles on Polymer Films and Their SERS Capabilities. *ACS Appl. Mater. Interfaces* **2013**, *5*, 8655-8662.
6. Faupel, F.; Zaporozhchenko, V.; Strunskus, T.; Elbahri, M., Metal-Polymer Nanocomposites for Functional Applications. *Adv. Eng. Mater.* **2010**, *12*, 1177-1190.
7. Kaune, G.; Ruderer, M. A.; Metwalli, E.; Wang, W.; Couet, S.; Schlage, K.; Röhlberger, R.; Roth, S. V.; Müller-Buschbaum, P., In Situ GISAXS Study of Gold Film Growth on Conducting Polymer Films. *ACS Appl. Mater. Interfaces* **2008**, *1*, 353-360.
8. Bigioni, T. P.; Lin, X.-M.; Nguyen, T. T.; Corwin, E. I.; Witten, T. A.; Jaeger, H. M., Kinetically driven self assembly of highly ordered nanoparticle monolayers. *Nat. Mater.* **2006**, *5*, 265-270.
9. Thiele, U.; Todorova, D. V.; Lopez, H., Gradient Dynamics Description for Films of Mixtures and Suspensions: Dewetting Triggered by Coupled Film Height and Concentration Fluctuations. *Phys. Rev. Lett.* **2013**, *111*, 117801.
10. Wong, H. C.; Cabral, J. T., Spinodal Clustering in Thin Films of Nanoparticle-Polymer Mixtures. *Phys. Rev. Lett.* **2010**, *105*, 038301.
11. Osborne, I.; Lavine, M.; Coontz, R., Looking Beyond Silicon. *Science* **2010**, *327*, 1595.

12. Mannhart, J.; Schlom, D. G., Oxide Interfaces—An Opportunity for Electronics. *Science* **2010**, *327*, 1607-1611.
13. Bang, J.; Jeong, U.; Ryu, D. Y.; Russell, T. P.; Hawker, C. J., Block Copolymer Nanolithography: Translation of Molecular Level Control to Nanoscale Patterns. *Adv. Mater.* **2009**, *21*, 4769-4792.
14. Herminghaus, S.; Jacobs, K.; Mecke, K.; Bischof, J.; Fery, A.; Ibn-Elhaj, M.; Schlagowski, S., Spinodal Dewetting in Liquid Crystal and Liquid Metal Films. *Science* **1998**, *282*, 916-919.
15. Lopes, W. A.; Jaeger, H. M., Hierarchical self-assembly of metal nanostructures on diblock copolymer scaffolds. *Nature* **2001**, *414*, 735-738.
16. Higgins, A. M.; Jones, R. A. L., Anisotropic spinodal dewetting as a route to self-assembly of patterned surfaces. *Nature* **2000**, *404*, 476-478.
17. Amarandei, G.; O'Dwyer, C.; Arshak, A.; Corcoran, D., The stability of thin polymer films as controlled by changes in uniformly sputtered gold. *Soft Matter* **2013**, *9*, 2695-2702.
18. Seemann, R.; Herminghaus, S.; Jacobs, K., Dewetting Patterns and Molecular Forces: A Reconciliation. *Phys. Rev. Lett.* **2001**, *86*, 5534-5537.
19. Xie, R.; Karim, A.; Douglas, J. F.; Han, C. C.; Weiss, R. A., Spinodal Dewetting of Thin Polymer Films. *Phys. Rev. Lett.* **1998**, *81*, 1251-1254.
20. Livage, J., Synthesis of polyoxovanadates via “chimie douce”. *Coord. Chem. Rev.* **1998**, *178–180, Part 2*, 999-1018.
21. Wong, H. C.; Cabral, J. o. T., Mechanism and Kinetics of Fullerene Association in Polystyrene Thin Film Mixtures. *Macromolecules* **2011**, *44*, 4530-4537.
22. Amarandei, G.; O'Dwyer, C.; Arshak, A.; Thiele, U.; Steiner, U.; Corcoran, D., Effect of Au Nanoparticle Spatial Distribution on the Stability of Thin Polymer Films. *Langmuir* **2013**, *29*, 6706-6714.
23. Livage, J., Vanadium pentoxide gels. *Chem. Mater.* **1991**, *3*, 578-593.
24. Riou, D.; Roubéau, O.; Férey, G., Evidence for the Solid State Structural Transformation of the Network-Type Decavanadate (NC<sub>7</sub>H<sub>14</sub>)<sub>4</sub>[H<sub>2</sub>V<sub>10</sub>O<sub>28</sub>] into a Lamellar Topology (NC<sub>7</sub>H<sub>14</sub>)[V<sub>4</sub>O<sub>10</sub>]. *Z. Anorg. Allg. Chem.* **1998**, *624*, 1021-1025.

25. Petkov, V.; Trikalitis, P. N.; Bozin, E. S.; Billinge, S. J. L.; Vogt, T.; Kanatzidis, M. G., Structure of V<sub>2</sub>O<sub>5</sub>·nH<sub>2</sub>O Xerogel Solved by the Atomic Pair Distribution Function Technique. *J. Am. Chem. Soc.* **2002**, *124*, 10157-10162.
26. Nomura, K.; Ohta, H.; Takagi, A.; Kamiya, T.; Hirano, M.; Hosono, H., Room-temperature fabrication of transparent flexible thin-film transistors using amorphous oxide semiconductors. *Nature* **2004**, *432*, 488-492.
27. Wang, L.; Yoon, M.-H.; Lu, G.; Yang, Y.; Facchetti, A.; Marks, T. J., High-performance transparent inorganic-organic hybrid thin-film n-type transistors. *Nat. Mater.* **2006**, *5*, 893-900.
28. Banger, K. K.; Yamashita, Y.; Mori, K.; Peterson, R. L.; Leedham, T.; Rickard, J.; Siringhaus, H., Low-temperature, high-performance solution-processed metal oxide thin-film transistors formed by a 'sol-gel on chip' process. *Nat. Mater.* **2011**, *10*, 45-50.
29. Sanchez, C.; Livage, J.; Henry, M.; Babonneau, F., Chemical modification of alkoxide precursors. *J. Non-Cryst. Solids* **1988**, *100*, 65-76.
30. Li, G.; Chu, C.-W.; Shrotriya, V.; Huang, J.; Yang, Y., Efficient inverted polymer solar cells. *Appl. Phys. Lett.* **2006**, *88*, 253503.
31. Nicholas, F.; Sean, M. P.; Mark, W. H.; Bharadwaja, S. S. N., Electrical properties of vanadium oxide thin films for bolometer applications: processed by pulse dc sputtering. *J. Phys. D: Appl. Phys.* **2009**, *42*, 055408.
32. Kumar, R. T. R.; Karunagaran, B.; Mangalaraj, D.; Narayandass, S. K.; Manoravi, P.; Joseph, M.; Gopal, V.; Madaria, R. K.; Singh, J. P., Room temperature deposited vanadium oxide thin films for uncooled infrared detectors. *Mater. Res. Bull.* **2003**, *38*, 1235-1240.
33. Gao, Y.; Cao, C.; Dai, L.; Luo, H.; Kanehira, M.; Ding, Y.; Wang, Z. L., Phase and shape controlled VO<sub>2</sub> nanostructures by antimony doping. *Energy Environ. Sci.* **2012**, *5*, 8708-8715.
34. Baddour-Hadjean, R.; Pereira-Ramos, J. P., New structural approach of lithium intercalation using Raman spectroscopy. *J. Power Sources* **2007**, *174*, 1188-1192.
35. Liu, J.; Wang, X.; Peng, Q.; Li, Y., Vanadium Pentoxide Nanobelts: Highly Selective and Stable Ethanol Sensor Materials. *Adv. Mater.* **2005**, *17*, 764-767.

36. Livage, J., Hydrothermal Synthesis of Nanostructured Vanadium Oxides. *Materials* **2010**, *3*, 4175-4195.
37. Jung, H.-M.; Um, S., Modification of electrical and surface properties of V<sub>2</sub>O<sub>3</sub> multilayer films on resin-impregnated highly oriented pyrolytic graphite composite substrates by shrinkage stress relaxation with chemical additives. *Thin Solid Films* **2013**, *548*, 98-102.
38. Kats, M. A.; Blanchard, R.; Zhang, S.; Genevet, P.; Ko, C.; Ramanathan, S.; Capasso, F., Vanadium Dioxide as a Natural Disordered Metamaterial: Perfect Thermal Emission and Large Broadband Negative Differential Thermal Emission. *Phys. Rev. X* **2013**, *3*, 041004.
39. Kats, M. A.; Sharma, D.; Lin, J.; Genevet, P.; Blanchard, R.; Yang, Z.; Qazilbash, M. M.; Basov, D. N.; Ramanathan, S.; Capasso, F., Ultra-thin perfect absorber employing a tunable phase change material. *Appl. Phys. Lett.* **2012**, *101*, 221101-221105.
40. Benkahoul, M.; Chaker, M.; Margot, J.; Haddad, E.; Kruzelecky, R.; Wong, B.; Jamroz, W.; Poinas, P., Thermochromic VO<sub>2</sub> film deposited on Al with tunable thermal emissivity for space applications. *Sol. Energy Mater. Sol. Cells* **2011**, *95*, 3504-3508.
41. Qazilbash, M. M.; Brehm, M.; Chae, B.-G.; Ho, P.-C.; Andreev, G. O.; Kim, B.-J.; Yun, S. J.; Balatsky, A. V.; Maple, M. B.; Keilmann, F.; Kim, H.-T.; Basov, D. N., Mott Transition in VO<sub>2</sub> Revealed by Infrared Spectroscopy and Nano-Imaging. *Science* **2007**, *318*, 1750-1753.
42. Schoiswohl, J.; Surnev, S.; Netzer, F. P.; Kresse, G., Vanadium oxide nanostructures: from zero- to three-dimensional. *J. Phys.: Condens. Matter* **2006**, *18*, R1-R14.
43. Kakiuchi, H.; Ohmi, H.; Yasutake, K., Atmospheric-pressure low-temperature plasma processes for thin film deposition. *J. Vac. Sci. Technol., A* **2014**, *32*,
44. Brinker, C. J.; Lu, Y.; Sellinger, A.; Fan, H., Evaporation-Induced Self-Assembly: Nanostructures Made Easy. *Adv. Mater.* **1999**, *11*, 579-585.
45. Glynn, C.; Thompson, D.; Paez, J.; Collins, G.; Benavente, E.; Lavayen, V.; Yutronic, N.; Holmes, J.; Gonzalez, G.; Odwyer, C., Large directional conductivity change in chemically stable layered thin films of vanadium oxide and a 1D metal complex. *J. Mater. Chem. C* **2013**, 5675-5684.
46. Kickelbick, G., Concepts for the incorporation of inorganic building blocks into organic polymers on a nanoscale. *Prog. Polym. Sci.* **2003**, *28*, 83-114.

47. O'Dwyer, C.; Lavayen, V.; Newcomb, S. B.; Santa Ana, M. A.; Benavente, E.; González, G.; Sotomayor Torres, C. M., Vanadate Conformation Variations in Vanadium Pentoxide Nanostructures. *J. Electrochem. Soc.* **2007**, *154*, K29-K35.
48. Silversmit, G.; Depla, D.; Poelman, H.; Marin, G. B.; De Gryse, R., Determination of the V2p XPS binding energies for different vanadium oxidation states (V5+ to V0+). *J. Electron Spectrosc. Relat. Phenom.* **2004**, *135*, 167-175.
49. Mendiáldua, J.; Casanova, R.; Barbaux, Y., XPS studies of V2O5, V6O13, VO2 and V2O3. *J. Electron Spectrosc. Relat. Phenom.* **1995**, *71*, 249-261.
50. So, S. K.; Choi, W. K.; Cheng, C. H.; Leung, L. M.; Kwong, C. F., Surface preparation and characterization of indium tin oxide substrates for organic electroluminescent devices. *Appl. Phys. A: Mater. Sci. Process.* **1999**, *68*, 447-450.
51. Gross, T.; Ramm, M.; Sonntag, H.; Unger, W.; Weijers, H. M.; Adem, E. H., An XPS analysis of different SiO2 modifications employing a C 1s as well as an Au 4f7/2 static charge reference. *Surf. Interface Anal.* **1992**, *18*, 59-64.
52. Wang, X. J.; Li, H. D.; Fei, Y. J.; Wang, X.; Xiong, Y. Y.; Nie, Y. X.; Feng, K. A., XRD and Raman study of vanadium oxide thin films deposited on fused silica substrates by RF magnetron sputtering. *Appl. Surf. Sci.* **2001**, *177*, 8-14.
53. Sanchez, C.; Livage, J.; Lucazeau, G., Infrared and Raman study of amorphous V2O5. *J. Raman Spectrosc.* **1982**, *12*, 68-72.
54. Driscoll, T.; Kim, H.-T.; Chae, B.-G.; Kim, B.-J.; Lee, Y.-W.; Jokerst, N. M.; Palit, S.; Smith, D. R.; Di Ventra, M.; Basov, D. N., Memory Metamaterials. *Science* **2009**, *325*, 1518-1521.
55. Su, Q.; Huang, C. K.; Wang, Y.; Fan, Y. C.; Lu, B. A.; Lan, W.; Wang, Y. Y.; Liu, X. Q., Formation of vanadium oxides with various morphologies by chemical vapor deposition. *J. Alloys Compd.* **2009**, *475*, 518-523.
56. Manning, T. D.; Parkin, I. P.; Clark, R. J. H.; Sheel, D.; Pemble, M. E.; Vernadou, D., Intelligent window coatings: atmospheric pressure chemical vapour deposition of vanadium oxides. *J. Mater. Chem.* **2002**, *12*, 2936-2939.



57. Vernardou, D.; Paterakis, P.; Drosos, H.; Spanakis, E.; Povey, I. M.; Pemble, M. E.; Koudoumas, E.; Katsarakis, N., A study of the electrochemical performance of vanadium oxide thin films grown by atmospheric pressure chemical vapour deposition. *Sol. Energy Mater. Sol. Cells* **2011**, *95*, 2842-2847.

**TOC Figure**

